Chapter 7

STUDIES ON MANGANESE BASED ORGANIC-INORGANIC HYBRID COMPOUNDS (OIHCs)

Abstract

In this chapter we discussed syntheses of two different manganese chlorides based OIHCs, $[(\text{anilinium})_2MnCl_4]_3.2C_2H_5OH$ (**23**) and $(\text{3-chloro anilinium})_8[MnCl_6]Cl_4$ (**24**). For compound **23** we observed the formation of thick bundles of crystals when aniline is treated with $MnCl_2$ in acidic ethanol solution. SEM images proved that these bundles (compound **23**) are about 100 μm thick due to the collection of very thin needle like crystals. $(C_6H_5NH_3)_2MnCl_4$ was crystallized in an orthorhombic space group *Cmca* having lattice constants a = 7.29 Å, b = 30.32 Å, c = 7.36 Å with volume of 1626.80 Å^3. Thermal analyses shows desorption of ethanol at 346.3 K and can be completely resorbed by exposure to ethanol vapors. These observations are supported by powder XRD study where change in cell volume close to 25 % was observed during desorption (**23-D**) analogues to narrow-pore (**NP**) ↔ large-pore (**LP**) forms, with shifting of 0k0 peaks, indicating change in interlayer distance. Absorption of ethanol molecules are not directly coordinated to compound but sit in pores which has been confirmed by SEM, mercury porosimetry and thermal studies. This reversible adsorption-desorption has also been observed for methanol, water as well as mixture of ethanol-water. DSC measurements have shown the strength of interactions and enthalpy of adsorption for the three polar solvents follows the order water < methanol < ethanol. Furthermore, single crystal XRD analysis on compound **24** have shown that it crystallized in triclinic space group *P-1* and has isolated metal chloride octahedra. Thermal studies on compound **24** have not shown any signature of adsorption-desorption.

7.1 Introduction

Designing of OIHCs or Metal-Organic framework (MOF) is emerging as a challenging field [1,2]. They have emerged as a very promising type of material because of their high porosity and specific surface area which has lead to technologically important applications concerned with catalysts [3,4,5], separation system [6], sensors [7], adsorbents [8,9] and gas storage materials [10,11,12] etc. But, apart from these MOFs and extended inorganic system where isolated inorganic systems are connected via organic linker can provide structural basis for many more physical properties than expected [13,14]. These materials have allowed the strategic coexistence of multiple technologically important properties within one material with generation/cleavage of coordination/hydrogen bonds associated with guest adsorption-desorption [15,16,17].

Metal halides on reaction with organic salts form a double salt [18]. These double salts can be synthesized in various structural formulas, as seen in earlier chapters. The most interesting related to present chapter is distorted perovskite type structures A_2MX_4. This type of compounds exhibit 2-D layer structures and as mentioned previously in this thesis it has varied technologically important properties such as semiconducting, magnetic and multiferroic properties [19,20]. Apart from this, these compounds can be seen as 'pore-prone' materials [21,22]. Because, pore size in these types of compounds can be tuned with (a) angles and geometry between M and X along with length of A; and (b) variety of hydrogen bonding patterns existed between A and X, which is yet to be explored. Thus, our preliminary goal is to study 'porous' organic-inorganic hybrid compounds.

Polar solvents like alcohols are attractive candidates as renewable, environmentally friendly sources of energy. Among them, the bio alcohols, ethanol and methanol can be used as fuels via their conversion to gasoline ("methanol-to-gasoline" or "methanol-to-olefins" processes) [23,24,25]. Much effort has been devoted to establish a rational design of structures for adsorption-desorption of these polar solvents but it is still a challenging issue, especially producing reversibility [9,26].

We have focused our preliminary research work on the syntheses of porous flexible compound, (anilinium)$_2$MnCl$_4$, which reversibly absorbs polar solvents such as ethanol, methanol and water. The structural flexibility and adsorption behavior is supported by powder XRD, TG/DTA measurement, DSC study, SEM analysis and mercury porosimetry measurements. In the process of 'modulating' and understanding the adsorption-desorption behavior by use of 3-chloroaniline (rather than aniline) we come across a new cluster compound, (3-chloro anilinium)$_8$[MnCl$_6$]Cl$_4$, is also discussed in this chapter.

7.2 Experimental

7.2.1 *Materials and Methods*

All chemicals and solvents used were of analytical grade reagents. Aniline (s. d. fine); 3-chloro aniline, manganese (II) chloride (Aldrich); conc. hydrochloric acid (qualigens) and ethyl alcohol (Baroda chemicals) were used whenever received.

7.2.2 Syntheses of OIHCs

Two new synthesized compounds are discussed in this chapter. A general methodology of their syntheses is mentioned in scheme-I.

Scheme-I

$$R\text{-}NH_3^+ Cl^- \xrightarrow[\text{Alcohol or Water}]{MnCl_2.2H_2O} (R\text{-}NH_3)_2MnCl_4$$

[Where, R = C_6H_5- (**23**), 3-Cl-C_6H_4- (**24**)]

In actual process, compounds, $[(C_6H_5NH_3)_2MnCl_4]_3.2C_2H_5OH$ (**23**) and (3-chloro anilinium)$_8$[MnCl$_6$]Cl$_4$ (**24**) were prepared in nitrogen environment by dissolving 2:1 ratio of OACSs [anilinium chloride 500.0 mg (3.858 mmol) and 3-chloro anilinium chloride 633.0 mg (3.858 mmol)] and manganese (II) chloride tetra hydrate 382.0 mg (1.929 mmol) in acidified distilled water. The solutions were refluxed for 4 hours and then dried completely using rotary evaporator. The powdered compounds were washed with ether and recrystallized by slow evaporation technique using ethanol. Fine needle like white crystals forming bundles for compound **23** and single crystal were obtained for compound **24** within 0 - 2 weeks.

Yield: 40 - 50 %

Compound **23**, when heated above 373 K losses ethanol molecule, we called this desorbed phase of **23** as **23-D**. **23-D** can be converted to **23-RE** by exposing it to ethanol vapors in a beaker for 0 - 5 days. We have prepared in a similar way **23-RM**, and **23-RW** as readsorbed methanol and water compounds.

7.3 Results and Discussions

7.3.1 General Discussion

The crystal structure and magnetism of the series (anilinium)$_2$MnCl$_4$ was initially reported by Daoud (1977) and El-Shaarawy (2000) [27,28]. Compound **23** crystallized in orthorhombic space group *Cmca* with lattice constants a = 7.29 Å, b = 30.32 Å, c = 7.36 Å, V = 1626.80 Å^3 and shows the antiferromagnetism in the temperature range of 80 K - 400 K. In these compounds $(NH_4)_2MnCl_4.2H_2O$, and (anilinium)$_2$MnCl$_4$ manganese (II) is hexacoordinated [29]. It is very common for hexacoordinated manganese (II) complexes to exhibit 4 + 2 coordination as a result of John-Teller effect with the distortion in manganese-ligand bonds. There are few examples where manganese has isolated as hexacoordinated (IV) complex K_2MnCl_6. Moews reported that $MnCl_6^{4-}$ ion in K_2MnCl_6 is octahedral, occupy at the corners and centers of the faces of the cubic unit cell, which are surrounded by eight K^+ ions at the corners of a cube [30]. Another example of manganese (II) compound in which Mn^{2+} ion surrounded by regular octahedral arrangement of chloride ions is K_4MnCl_6 [31].

We observed faint red colored crystals of (3-chloro anilinium)$_8$[MnCl$_6$]Cl$_4$, compound **24**, is also discussed in this chapter.

7.3.2 FT-IR Spectra

Analytical data for the compounds **23** and **24** are given below.

23: FT-IR (KBr) 3431 (vs), 3007 (vs), 2564 (s), 1882 (m), 1611 (s), 1571 (s), 1479 (vs), 1329 (w), 1292 (w), 1191 (w), 1089 (s), 1032 (m), 746 (vssh), 682 (vssh), 528 (s) and 471 (s) cm^{-1}.

24: FT-IR (KBr) 2976 (vs), 2897 (vs), 2568 (s), 2385 (w), 1877 (m), 1597 (s), 1560 (s), 1490 (s), 1478 (vssh) 1445 (s), 1303 (m), 1281 (m), 1098 (m), 1079 (s), 1051 (m), 1001 (w), 872 (s), 779 (ssh), 674 (ssh), 528 (ssh), and 440 (m) cm^{-1}.

FT-IR spectra shows asymmetric stretching modes of N-H ($-NH_3^+$ group) shifted at 3007 - 2976 cm^{-1} and 2897 - 2564 cm^{-1} with respect to OIHCs indicating breaking of continuous series of hydrogen bond. The other N-H ($-NH_3^+$ group) deformation modes and rocking modes were observed at 1611 - 1597 cm^{-1} and 1571 - 1490 cm^{-1} respectively. The vibrational modes observed between 1329 - 1281 cm^{-1} were due to aromatic C-N stretching. Other modes which provide vital information about the C-H aromatic ring out of plane deformation signifies five and three hydrogen adjacent position at 746 cm^{-1}, 682 cm^{-1} and 779 cm^{-1} for compounds **23** and **24** respectively. Vibrational mode is also observed at 3431 cm^{-1} for compound **23** due to O-H stretching. FT-IR spectra of OIHCs are illustrates in Figure 7.1.

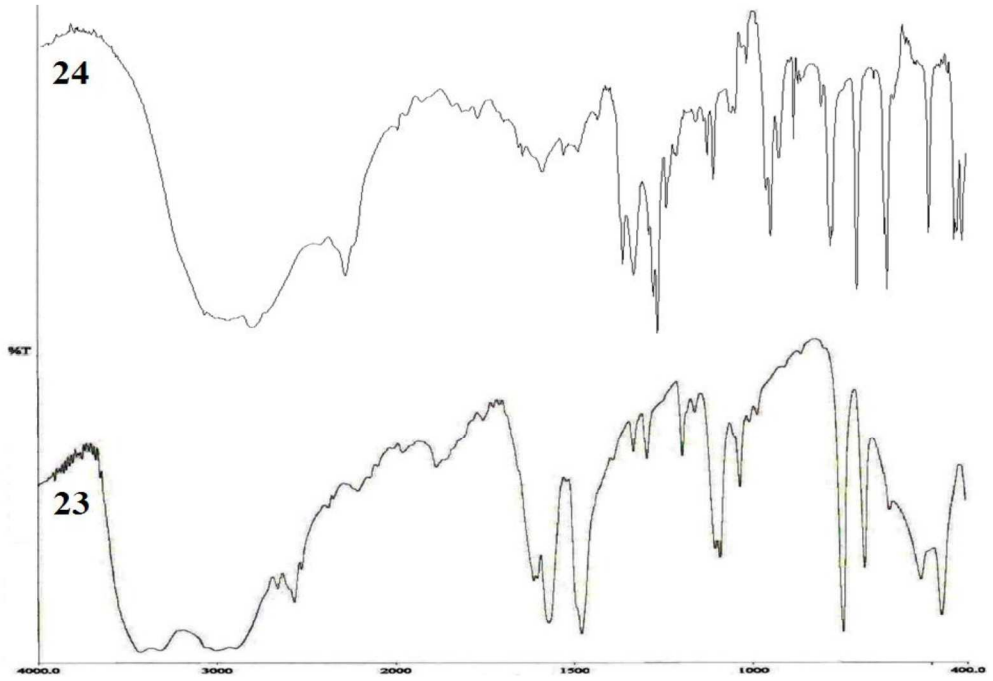

Figure 7.1 FT-IR spectra of compounds **23** and **24**.

7.3.3 Elemental Analyses

The elemental analyses were consistent with the formulae A_2MnCl_4. *Anal.* Ref. sulfanilamide: Found (calc.) %; C, 41.85 (41.81); H, 4.68 (4.65); N, 15.26 (16.25).

$[(C_6H_5NH_3)_2MnCl_4]_3.2C_2H_5OH$ (**23**)**:** Found (calc.) %; C, 38.42 (38.53); H, 3.41 (3.37); N, 6.67 (6.74). $(3\text{-}Cl\text{-}C_6H_4NH_3)_2[MnCl_6]Cl_4$ (**24**)**:** Found (calc.) %; C, 39.98 (40.09); H, 3.78 (3.89); N, 7.64 (7.79).

7.3.4 Thermal Analyses

7.3.4.1 Thermo gravimetry/Differential Thermal Analysis (TG/DTA)

TG/DTA of OIHCs was performed on the powdered compounds. Figure 7.2 shows the thermal analyses curve for compounds **23** and **24**. Compound **23** represent different degradation pathways as compared to compound **24** as tabulated below.

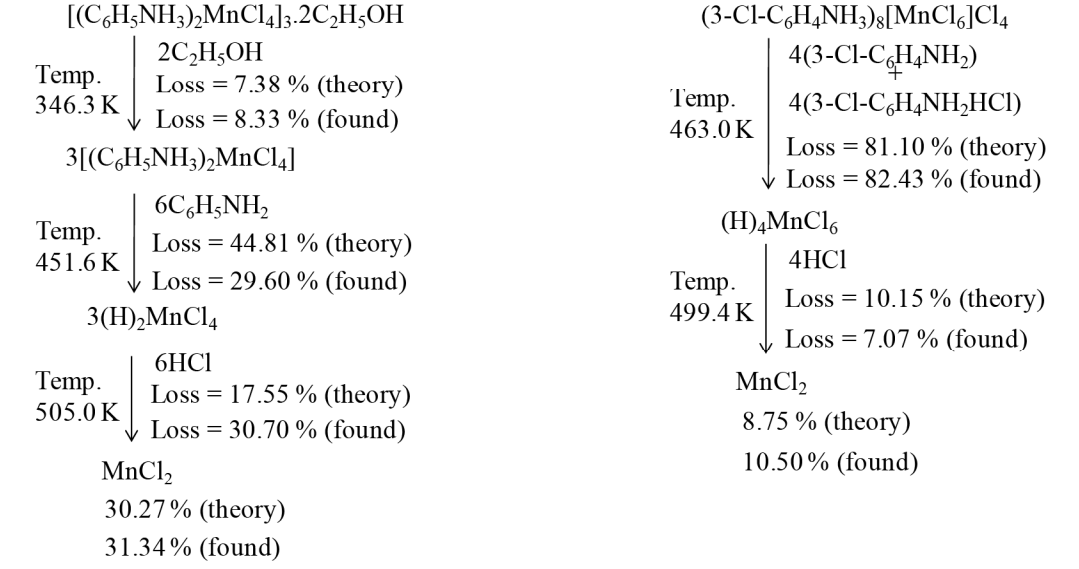

Figure 7.2 (a) TG/DTA of compound **23** shows the first weight loss at 346.3 K (onset at 338.0 K with 8.12 % loss) then at 451.6 K (29.14 % loss) and 505.0 K (30.25 % loss). Calculated first weight loss comes very close to the evaporation value of two ethanol molecules per three formula units. Calculation of second weight loss comes very close to the evaporation of two molecules of aniline ($C_6H_5NH_2$) per formula unit but it is not completely evaporated at this temperature and shows the continuous weight loss up to 456.0 K. The third weight loss comes close to the value for the evaporation of two molecules of hydrochloric acid per formula unit and the remaining weight corresponds to manganese (II) chloride ($MnCl_2$). It is clear that the first weight loss is due to ethanol which is not coordinated with the metal. Therefore, TG/DTA

measurements for compound **23-D** shows absence of first weight lost in this temperature range see Figure 7.2 (b). While compound **23-RE** shows presence of first weight lost at 338.8 K which is expected for ethanol molecules see Figure 7.2 (c).

On the other hand compound **24** shows only two weight loss, first weight loss at 463.0 K (82.43 % loss) and second weight loss at 499.4 K (7.07 % loss). Calculated first weight loss comes very close to the evaporation of four moles of 3-chloro aniline and four moles of 3-chloro anilinium chloride per formula unit. After the loses of 3-chloro aniline and four moles of 3-chloro anilinium chloride, $(H)_4MnCl_6$ is left. At HT it again loses hydrochloric acid leaving behind $MnCl_2$. Calculation of second weight loss comes very close to the evaporation of four moles of HCl per formula unit as shown in Figure 7.2 (d).

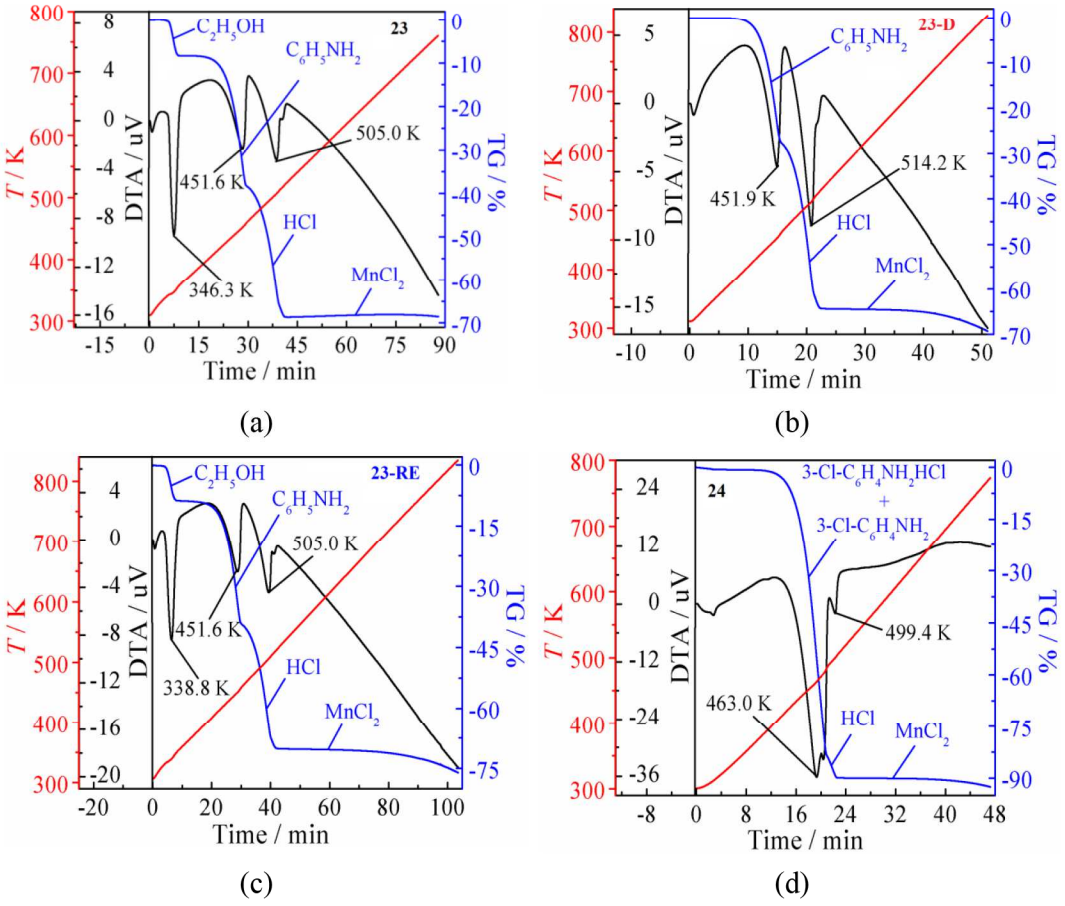

Figure 7.2 TG/DTA curves for compounds **23** (a); **23-D** (b); **23-RE** (c) and **24** (d).

Thermal experiments were revised to investigate number of time desorption-resorption features for compound **23-D** when brought in contact with ethanol. DTA

signals for removal of ethanol from compounds **23-RE**, **23-RE-1** and **23-RE-2** occurs at similar temperature with decrease in energy suggesting reversibility of these phenomena [Figure 7.3 (a)].

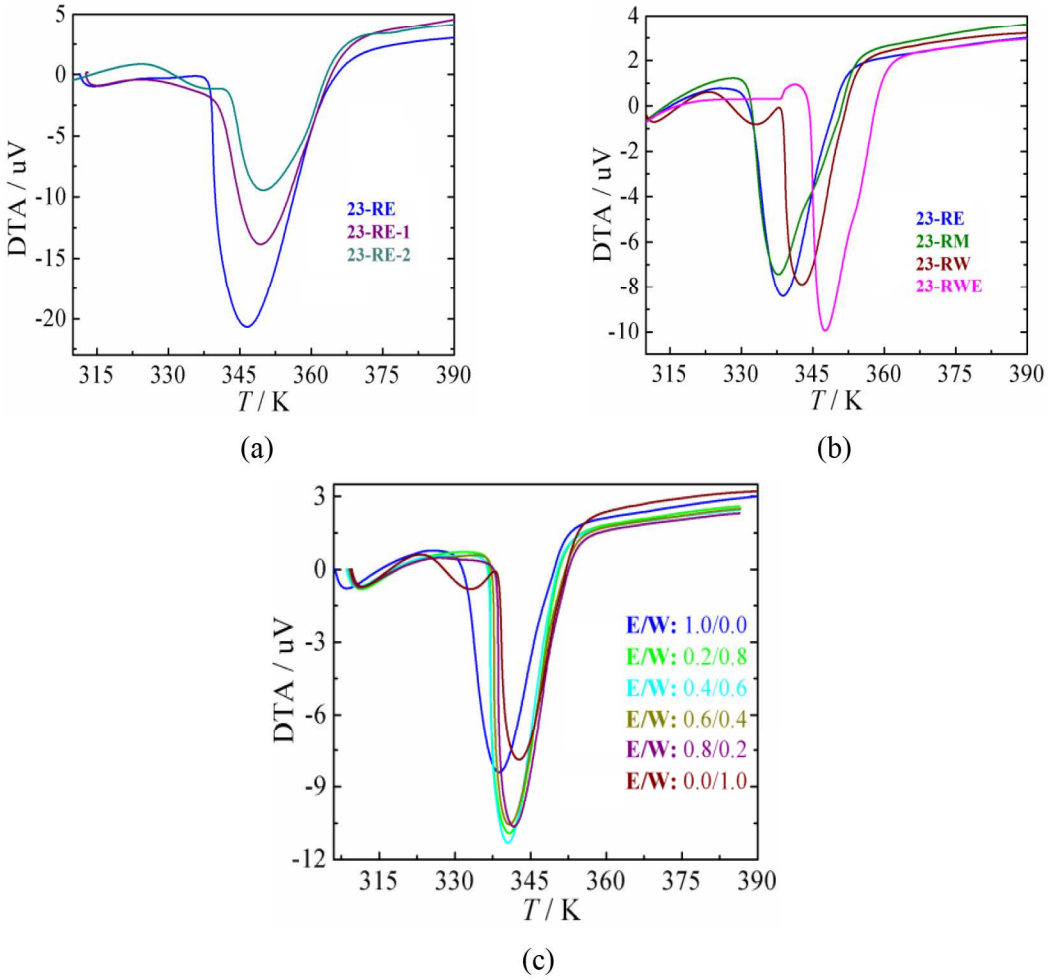

Figure 7.3 DTA curves of compounds **23-RE**, **23-RE-1**, **23-RE-2** (a), showing peak at constant temperature; DTA curves of compounds **23-RE**, **23-RM**, **23-RW**, **23-RWE** (b) and DTA of desorption after placing in different **E/W** vapor mixture (c).

If ethanol is showing adsorption-desorption behavior, then is it possible to use other polar solvents? Therefore, compound **23-D** was exposed to methanol, $[(C_6H_5NH_3)_2MnCl_4].CH_3OH$ (**23-RM**), water, $[(C_6H_5NH_3)_2MnCl_4].2H_2O$ (**23-RW**), and water then ethanol $[(C_6H_5NH_3)_2MnCl_4]_3.2C_2H_5OH$ (**23-RWE**). In these cases also as anticipated first weight loss due to methanol, water and ethanol have been observed (Figure 7.4).

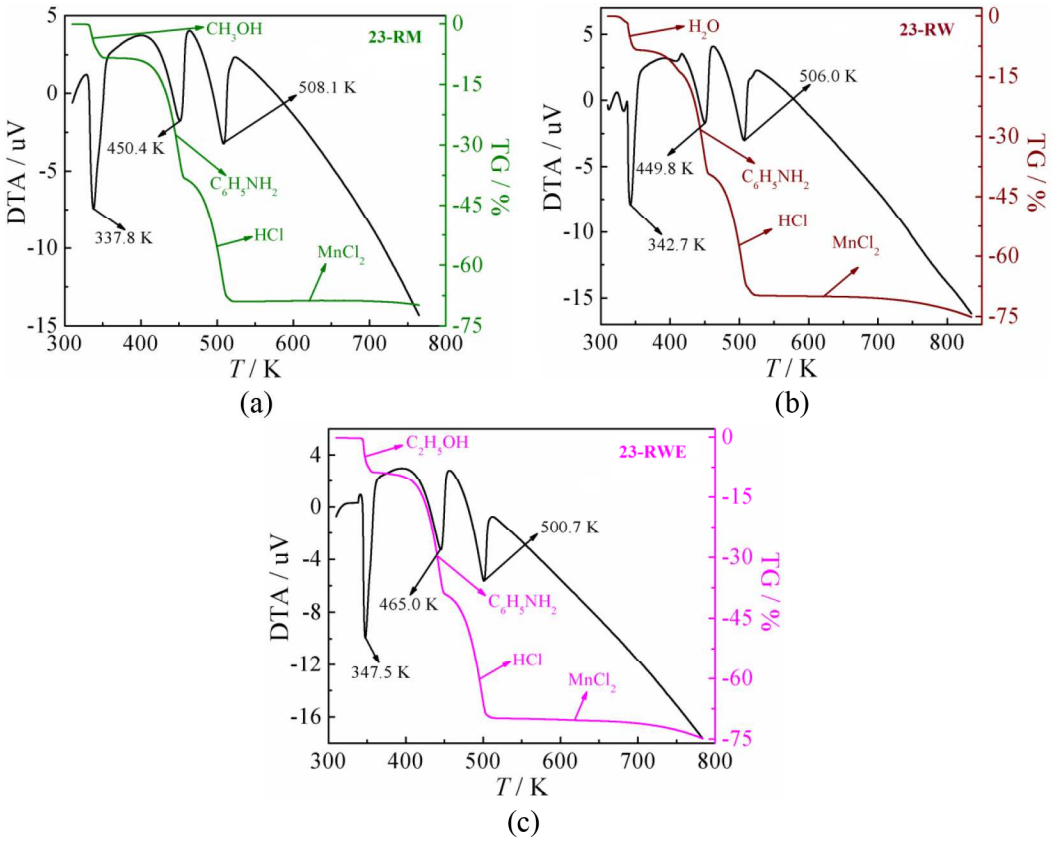

Figure 7.4 TG/DTA curve of compounds **23-RM** (a); **23-RW** (b) and **23-RWE** (c).

Furthermore, the selectivity adsorption of polar vapor for compound **23-D** compound particularly for ethanol and water, initially was brought in contact of water vapor atmosphere in closed packed beaker for two days **23-RW**, then was brought it in contact of ethanol vapor atmosphere for two days **23-RWE**, as shown in Figure 7.3 (b). DTA for the desorption of water shows two peaks, one initial small peak at 333.17 K and other main peak at 342.7 K while desorption of pure ethanol and water then ethanol revealed only one peak at 338.8 K and 347.5 K, respectively and it supported the selectivity adsorption of polar vapor of DSC experiments. TG/DTA measurements were also performed with ethanol/water vapors mixture. Compound **23-D** when initially brought in contact with different ethanol/water vapor mixture atmosphere, Figure 7.3 (c), the shape of DTA signals of different ethanol/water vapor mixture largely resembles those previously observed in case of desorption of pure ethanol. This indicates that ethanol vapors are well fitted into the pore channel as compared to water vapors.

7.3.4.2 Differential Scanning Calorimetry (DSC)

DSC measurement on compound **23** shows an endothermic peak at 357.01 K while heating, corresponds to desorption of ethanol from the **NP** (next section will discuss the narrow size of the pores) form which are not observed for compound **23-D**. On the other hand, compound **23-RE** shows an endothermic peak at 350.78 K which is slightly lower than compound **23**. This may be due to easiness of desorption during resorption as shown in Figure 7.5 (a).

When adsorption-desorption is repeated several times (**RE-1**, **RE-2**) as shown in Figure 7.5 (b), we observed small changes in peak positions and intensity. This later effect may be due to the role played by different kinetic aspect of adsorptions, since was not distinct in the TG/DTA measurements.

We conducted a comparative desorption behavior of compound **23** with respect to ethanol, methanol and water using DSC studies. Desorption of water shows shoulder just before onset of transition, suggesting slight sluggish removal of water [Figure 7.5 (c)]. Enthalpy values obtained from DSC peaks confirms the strength of interactions follows a sequence methanol < water < ethanol (Table 7.1), similar to literature values for porous chromium (III) terephthalate MIL-53(Cr), complex [32]. Thus, DSC examination on compound **23** indicates that only ethanol molecules from the vapor are well fitted into the exploded pore channels over methanol and water.

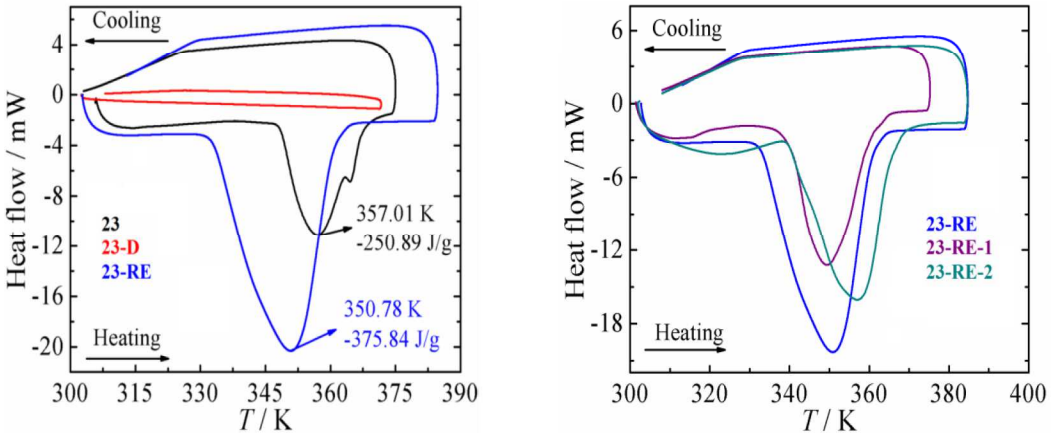

(a) (b)

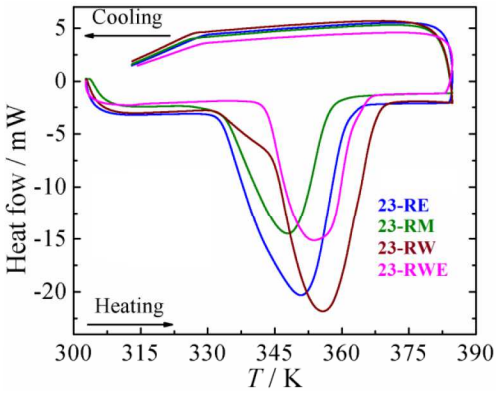

(c)

Figure 7.5 DSC plots for compounds **23**, **23-D** and **23-RE** (a); for compounds **23-RE**, **23-RE-1** and **23-RE-2** (b), showing transition nearly at same temperature indicating adsorption-desorption is completed reversibly; and resolvated compounds with different vapor **23-RE**, **23-RM**, **23-RW** and **23-RWE** (c).

We also conducted a comparative desorption behavior of compound **23-D** with respect to ethanol and water using DSC study. We observed that when compound **23-RW** is exposed to ethanol vapors only partial replacement of water molecules with ethanol molecules takes place, as predicted by theory for porous compounds [9]. Here, DSC peak and enthalpy (-363.98 J g^{-1}) of desorption appears between desorption peak of pure ethanol and water peak as shown in Figures 7.5 (c). This suggested that ethanol vapor replacing water molecule from porous manganese (II) anilinium framework which is already sitting there but ethanol vapors have not removed water molecule completely.

When DSC studies were performed to follow the adsorption features on ethanol/water vapors mixture compound **23-D** initially brought in contact with different ethanol/water vapor mixture atmosphere. DSC signals of different ethanol/water vapor mixtures are similar to those previously observed in case of desorption of pure ethanol [Figure 7.6 (a)]. These experiments are strongly supported by TG/DTA measurements [Figure 7.3 (c)].

To understand percentage adsorbance of compound **23-D** for polar solvents, compound **23-D** was placed in ethanol moisture and weight measured at different intervals of time. It shows initially absorption increase rapidly to maximum 40 % and saturated after 120 min as shown in Figure 7.6 (b).

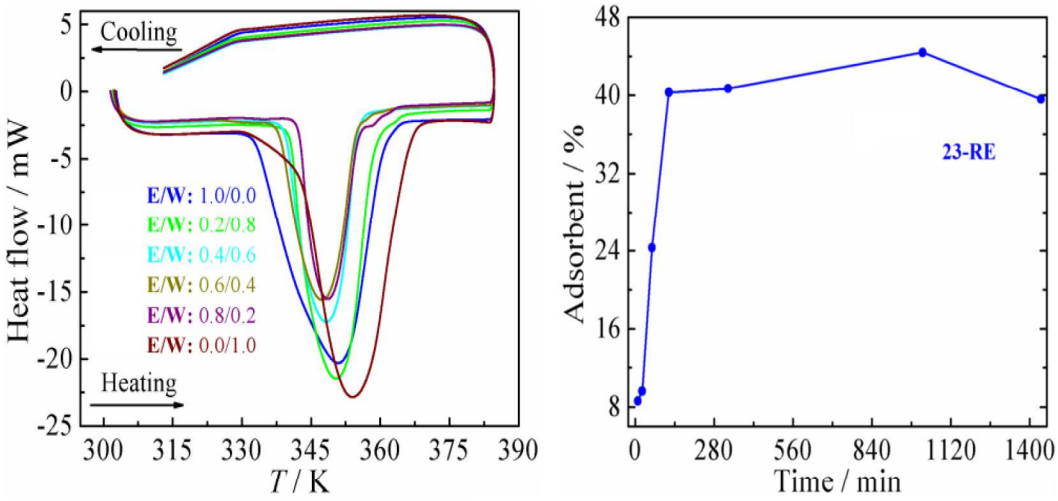

(a) (b)

Figure 7.6 DSC plots of desorption after placing in different **E/W** vapor mixture (a) and Plot of moisture adsorption capacity in compound **23-D** time versus absorbance % (b).

Table 7.1 Enthalpy of compound **23-RE**, **23-RM**, **23-RW** and **23-RWE**

Solvents	Enthalpy [J g^{-1}]
23-RE	350.78 K (-375.84)
23-RM	345.72 K (-352.96)
23-RW	354.01 K (-358.50)
23-RWE	354.42 K (-363.98)

We have also performed DSC measurements for compound **24** in the temperature range 173 K - 403 K. DSC measurement did not show any transition in this temperature range.

7.3.5 Crystal Structure

7.3.5.1 Powder X-ray Diffraction

$(Anilinium)_2MnCl_4$ crystallized in orthorhombic space group *Cmca* with lattice constants a = 7.29 Å, b = 30.32 Å, c = 7.36 Å and V = 1626.80 $Å^3$. The structure

consists of layered corner sharing octahedra of [$MnCl_6$] sandwiched between anilinium ions characteristic of A_2MX_4 family [28]. Figure 7.7 (a) shows powder XRD pattern for compound **23** along with its ethanol desorbed compound **23-D** and resorbed phase compound **23-RE**. These powder patterns were indexed in orthorhombic crystal system using powder X5 software which verifies the structural changes taking place during an adsorption-desorption process (Table 7.2). The data for compounds **23-D** and **23-RE** were collected after placing the compound **23** in oven at 378.0 K for 1 hour and exposing compound **23-D** in a closed beaker containing ethanol at RT for 5 days respectively. The powder XRD study for compound **23** and the resolvated in ethanol solvent (compound **23-RE**) shows almost similar pattern indicating resorption in compound **23** is completely reversible [Figure 7.7 (a)]. The powder XRD pattern for desolvation compound **23-D** shows apparently shift in 0k0 peaks corresponding to change in interlayer spacing. The interlayer spacing peaks at 030 and 050 in compound **23** are shifted to 020 and 040 in compound **23-D** indicating decreasing of interlayer space after desorption [33]. The diffraction peaks revealed reversibility of resorption after regenerates interlayer peaks 030 and 050 in compound **23-RE**. The powder XRD peak 101 present in compound **23** also shows regeneration with resorption in compound **23-RE** indicating the compound returned to its original form. The intensity of the peaks in compound **23-RE** are less intense as compared to compound **23** indicating a slight decrease in the structural order in adsorption-desorption process. This is due to either a small degree of pillar disorder or an incomplete resorption of the compound. The powder XRD studies for compounds **23-RM** and **23-RW** also show the reversibility of peaks when exposed to different polar solvents such as methanol and water [Figure 7.7 (b)]. The observed changes in the diffraction of 0k0 peaks indicates interlayer space is shifting during the adsorption-desorption process. The change in cell volume appreciably from compound **23** (1933.621 $Å^3$) to compound **23-D** (1797.395 $Å^3$) confirm observed structural changes during desorption is completely reverse after absorption. This generated an important question *i.e.*, whether the observed desorption-resorption may be due to structural change or presence of porosity in the structure or both. To understand this we carried out SEM and mercury porosimetry measurements, see next section.

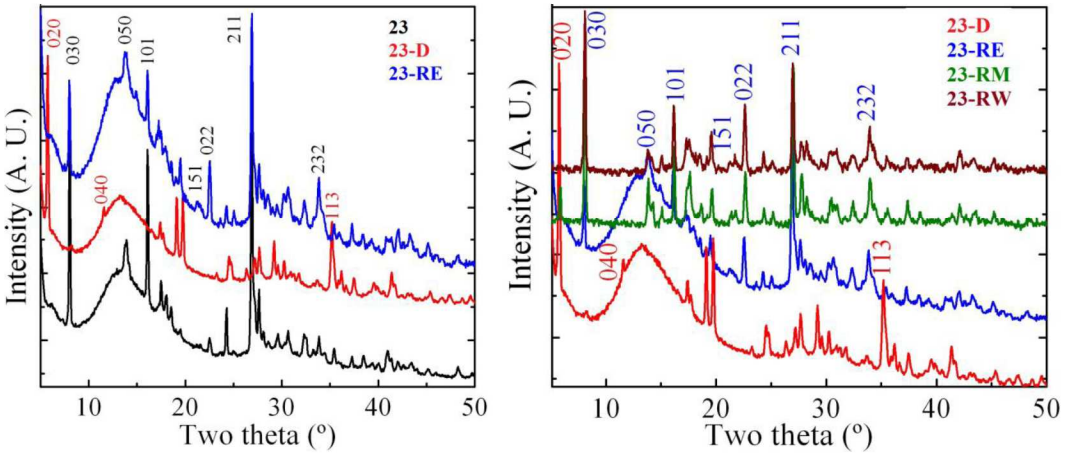

Figure 7.7 Comparison of powder XRD diagrams for compounds **23**, **23-D** and **23-RE** (a); and compounds **23-D**, **23-RE**, **23-RM** and **23-RW** (b), illustrate reversibility during desorption-resorption.

Table 7.2 Crystal data and structure index parameters for compounds **23**, **23-D**, **23-RE**, **23-RM** and **23-RW**

	23	**23-D**	**23-RE**	**23-RM**	**23-RW**
Formula	$[(An)_2MnCl_4]_3.$ $2C_2H_5OH$	$(An)_2MnCl_4$	$[(An)_2MnCl_4]_3.$ $2C_2H_5OH$	$[(An)_2MnCl_4].$ CH_3OH	$[(An)_2MnCl_4].$ $2H_2O$
Molecular weight	1247	385	1247	417	421
Temperature K	298	298	298	298	298
Crystal system	Orthorhombic	Orthorhombic	Orthorhombic	Orthorhombic	Orthorhombic
Lattice Type	*P*	*P*	*P*	*P*	*P*
a Å	7.33	7.33	7.33	7.38	7.23
b Å	32.15	30.15	32.15	31.79	32.15
c Å	8.19	8.19	8.19	8.13	8.19
β (°)	90	90	90	90	90
V Å^3	1933.621	1797.395	1928.034	1917.397	1899.312
Radiation (λ)	1.54184	1.54184	1.54184	1.54184	1.54184
2*θ* range (°)	5 – 50	5 - 50	5 - 50	5 - 50	5 - 50
N. reflections	1701	1701	1701	1541	1541
R factor	0.00307	0.00315	0.00356	0.00395	0.00273

7.3.5.2 Structural Characterization

Simple optical microscope revealed conversion of shiny transparent crystals of compound **23** to opaque after desolvation, compound **23-D**, as shown in Figure 7.8 (a). SEM images represent that these crystals are of size 100 μm thick, and is nothing but a 'collection' of very thin needles, less than 10 μm thick needles, stacking as shown in Figure 7.8 (b). When ethanol is desorbed, compound **23-D**, the porous network of 3 - 4 μm gets exposed which after resorption gets filled. Thus, we can say that the adsorption-desorption occurs due to gate opening-closing of compound **23** from a **NP** to **LP** and again **NP** form. The mercury porosimetry measurements results for compounds **23** and **23-D** shows materials exhibit change in pore size from 0.071448 μm to 3.717309 μm respectively. The cell volume of compound **23** (**NP**) changes from 9.7 % to 35.4 % when it is converted to compound **23-D** (**LP**) that is during adsorption-desorption of ethanol vapors.

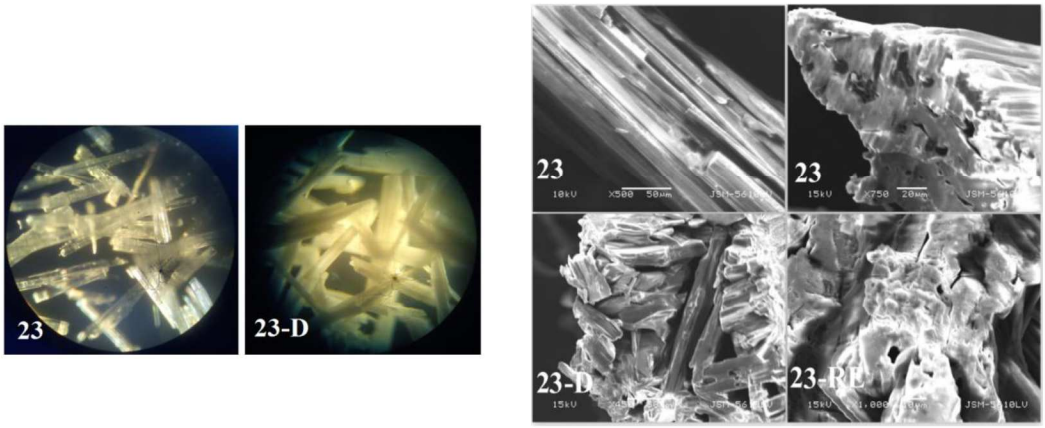

(a) (b)

Figure 7.8 Images of simple optical microscope shows shiny transparent crystals of compound **23**, becomes opaque on desolvation, compound **23-D** (a); and SEM images comparison of porous materials for compounds **23**, **23-D** and **23-RE** (b), indicate completely reversible adsorption-desorption.

7.3.5.3 Single Crystal X-ray Diffraction

A summary of crystallographic data and structure solutions for compound **24** are given in Table 7.3. Figure 7.9 shows the asymmetric unit of compound **24**.

Table 7.3 Crystallographic data and structure refinements for compound **24**

Empirical formula	$C_{48}H_{56}Cl_{18}MnN_8$	Crystal size (mm^3)	0.32×0.30×0.29
Formula weight	1438.11	$F(000)$	756
T (K)	293	2θ range (°)	3.24–29.20
Wavelength (Å)	0.71073	Index ranges	-11 ≤ h ≤ 11,
Crystal system	Triclinic		-18 ≤ k ≤ 18,
Space group	*P-1*		-17 ≤ l ≤ 13
a (Å)	8.6939(17)	Reflections collected	11542
b (Å)	13.936(2)	Independent reflections	7167 [R_{int} = 0.0596]
c (Å)	14.121(3)	Completeness to θ = 25.24°	98.0 %
α (°)	81.629(15)	Goodness-of-fit on F^2	1.057
β (°)	72.611(17)	Data / restraints / parameters	7167 / 0 / 341
γ (°)	77.374(15)	Final R indices [I>2σ(I)]	$R1$ = 0.099,
V ($Å^3$)	1587.3(5)		w$R2$ = 0.3125
Z	1	R indices (all data)	$R1$ = 0.1723,
D_{calc} (Mg/m^3)	1.504		w$R2$ = 0.2400

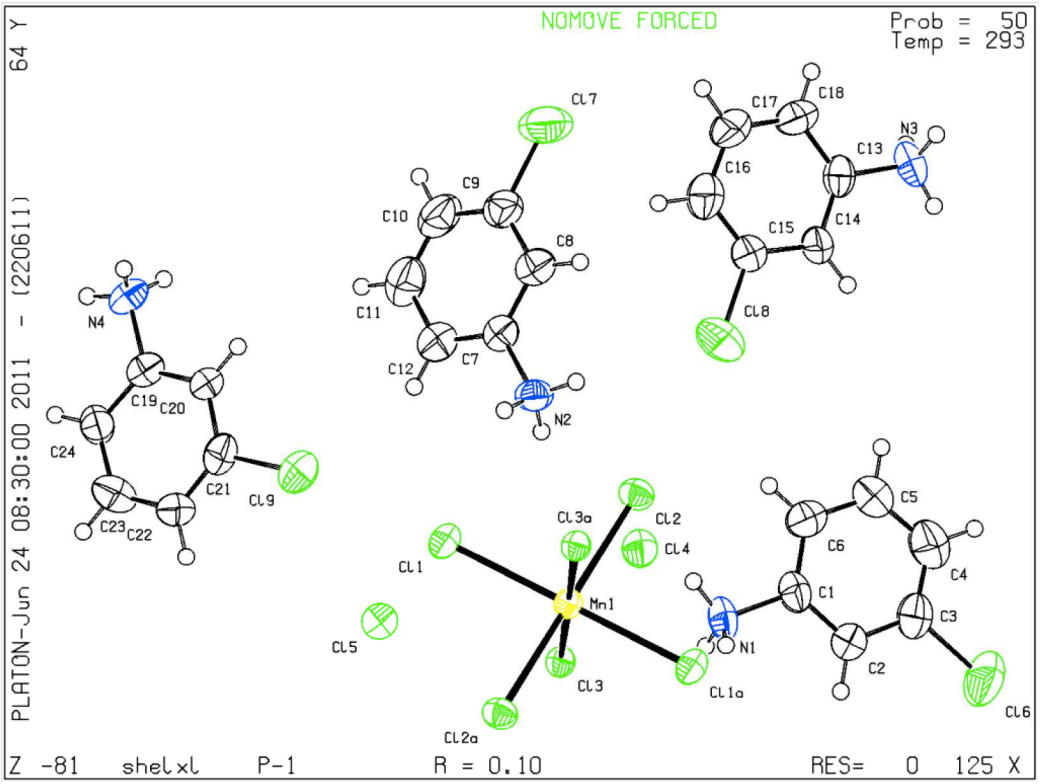

Figure 7.9 The structure of compound **24** showing the asymmetric units.

Single crystal XRD study reveals that compound **24** crystallized in triclinic space group *P-1* with unit cell dimensions a = 8.6939(17) Å, b = 13.936(2) Å, c = 14.121(3) Å, α = 81.629(15)º, β = 72.611(17)º, γ = 77.374(15)º, V = 1587.3(5) Å^3 and Z = 1. The coordination about the discrete $(MnCl_6)^{4-}$ ion is tetragonally compressed octahedron with bond distances Mn-Cl(1) = 2.590(2) Å, Mn-Cl(2) = 2.597(2) Å and Mn-Cl(3) = 2.471(2) Å. The two short bond distances are seen for manganese-chloride bonds but the remaining four bond distances are remarkably long for 4 + 2 coordination. The Cl(1)-Mn-Cl(1a), Cl(2)-Mn-Cl(2a) and Cl(3)-Mn-Cl(3a) angles are strictly 180.00(7)º and remaining Cl(*i*)-Mn-Cl(*j*) angles differ from 90º by ±1º. Bond distances and bond angles for $MnCl_6^{4-}$ anion are given in Table 7.4. Chlorine of the aromatic ring and nitrogen atom of the protonated amino group is lying in the plane. Single crystal X-ray structure determination on compound **24** revealed the presence of 3-chloro anilinium ions, $MnCl_6^{4-}$ units and uncoordinated chloride ions. A stereo view that shows the arrangement of these ions in the unit cell is shown in Figure 7.10.

Table 7.4 Bond distances, angles and metal-metal distances for compound **24** [Å and °]

Bond distance [Å]			
Mn(1)-Cl(1)	2.590(2)	Mn(1)-Cl(3a)	2.4707(18)
Mn(1)-Cl(2)	2.597(2)	Mn(1)-Cl(2a)	2.597(2)
Mn(1)-Cl(3)	2.4707(18)	Mn(1)-Cl(1a)	2.590(2)
Bond Angle [°]			
Cl(3)-Mn(1)-Cl(3a)	180.00(6)	Cl(1a)-Mn(1)-Cl(2a)	91.00(7)
Cl(3)-Mn(1)-Cl(1a)	89.79(7)	Cl(1)-Mn(1)-Cl(2a)	89.01(7)
Cl(3a)-Mn(1)-Cl(1a)	90.21(7)	Cl(3)-Mn(1)-Cl(2)	90.66(7)
Cl(3)-Mn(1)-Cl(1)	90.21(7)	Cl(3a)-Mn(1)-Cl(2)	89.34(7)
Cl(3a)-Mn(1)-Cl(1)	89.79(7)	Cl(1a)-Mn(1)-Cl(2)	89.01(7)
Cl(1)-Mn(1)-Cl(1a)	180.00(7)	Cl(1)-Mn(1)-Cl(2)	90.99(7)
Cl(3)-Mn(1)-Cl(2a)	89.35(7)	Cl(2)-Mn(1)-Cl(2a)	180.00(7)
Cl(3a)-Mn(1)-Cl(2a)	90.66(7)		
Metal-metal distance [Å]			
Mn-Mn (inter)	14.121(3)	Mn-Mn (intra)	8.694(2)
Axial Cl···Cl	9.753(4)	Equatorial Cl···Cl	3.753(3)

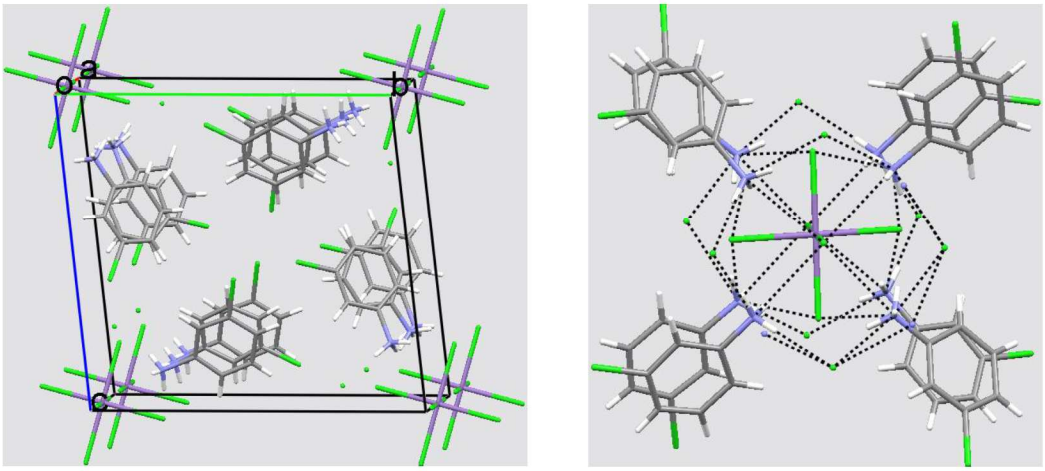

Figure 7.10 Stereo view that illustrates the packing of ions in the unit cell for compound **24**.

In practice, OIHCs generally formed layers of corner-sharing metal halide MX_4^{2-} octahedra as an inorganic component and they are separated by various organic cations. The organic ions are perpendicular to the metal halide layers. But in this case octahedral $MnCl_6^{4-}$ units gives the isolated structure of the inorganic component. The $MnCl_6^{4-}$ anions are at the corners center of the faces of the unit cell, surrounded by eight 3-chloro anilinium cations and ten chloride free ions (Figure 7.10), which is isostructural with the compounds previous reported in the literatures $(3\text{-}X\text{-}C_6H_4NH_3)_2[MCl_6]Cl_4$ (X = Cl, Br, I and M = Cu, Ni) [34,35,36]. This is stabilized by different kinds of non-covalent interactions such as hydrogen bond.

CCDC No. 882843 contains the crystallographic data for the compound **24**. This data can be obtained free of charge via http://www.ccdc.cam.ac.uk/conts/retrieving.html, or from the Cambridge Crystallographic Data Centre, 12 Union Road, Cambridge CB2 1EZ, UK; fax: (+44) 1223 336 033; or e-mail: deposit@ccdc.cam.ac.uk.

7.4 Conclusion

- We have synthesized two different OIHCs; bundle shaped thin needle like crystals of porous manganese (II) anilinium framework, $[(An)_2MnCl_4]_3.2C_2H_5OH$, and needle like single crystals of $(3\text{-}Cl\text{-}C_6H_4NH_3)_2[MnCl_6]Cl_4$.

- Thermal analyses have shown desorption of ethanol can be completely resorbed, by expose to ethanol vapors. These observations are evident from powder XRD study, where 25 % change in cell volume has been correlated to change in **NP** ↔ **LP** forms, with shifting of 0k0 peaks, indicating change in interlayer distance, and conformed by SEM and mercury porosimetry.
- SEM images conclude that these bundles (around 100 μm thick) have pore forming channels with diameter from 14 - 16 μm in the desolvated phase, compound **23-D**.
- The reversible adsorption-desorption have been examined for ethanol, methanol, water and water then ethanol. DSC examination have shown the strength of interactions and enthalpy of adsorption for the three polar solvents follows sequence, water < methanol < ethanol.
- DSC study on compound **24** does not show any information up to the degradation temperature.
- Single crystal XRD study on compound **24** showed it crystallized in triclinic space group *P-1* and have isolated structure of $MnCl_4^{2-}$.

References

[1] E. D. Bloch, D. Britt, C. Lee, C. J. Doonan, F. J. Uribe-Romo, H. Furukawa, J. R. Long, O. M. Yaghi, *J. Am. Chem. Soc.* **2010**, *132*, 14382-14384.

[2] J. R. Long, O. M. Yaghi, *Chem. Soc. Rev.* **2009**, *38*, 1213-1214.

[3] W. Lin, *Top. Catal.* **2010**, *53*, 869-875.

[4] L. Yan, X. Weimin, C. Yong, *Adv. Mater.* **2010**, *22*, 4112-4135.

[5] D. Britt, C. Lee, F. J. Uribe-Romo, H. Furukawa, O. M. Yaghi, *Inorg. Chem.* **2010**, *49*, 6387-6389.

[6] B. Chen, S. Xiang, G. Qian, *Acc. Chem. Res.* **2010**, *43*, 1115-1124.

[7] S. A. Sapchenko, D. G. Samsonenko, D. N. Dybtsev, M. S. Melgunov, V. P. Fedin, *Dalton Transactions* **2011**, *40*, 2196-2203.

[8] A. Nalaparaju, X. S. Zhao, J. W. Jiang, *J. Phys. Chem. C* **2010**, *114*, 11542-11550.

[9] D. Saha, S. Deng, Z. Yang, *J. Porous Mater.* **2009**, *16*, 141-149.

[10] J. Getzschmann, I. Senkovska, D. Wallacher, M. Tovar, D. Fairen-Jimenez, T. Düren, J. M. van Baten, R. Krishna, S. Kaskel, *Micropor. Macropor. Mater.* **2010**, *136*, 50-58.

[11] Z. Chen, S. Xiang, T. Liao, Y. Yang, Y. -S. Chen, Y. Zhou, D. Zhao, B. Chen, *Cryst. Growth Des.* **2010**, *10*, 2775-2779.

[12] P. O. Vasiliev, Z. Shen, R. P. Hodgkins, L. Bergström, *Chem. Mater.* **2006**, *18*, 4933-4938.

[13] A. K. Cheetham, C. N. R. Rao, *Science* **2007**, *318*, 58-59.

[14] J. L. Mohanan, I. U. Arachchige, S. L. Brock, *Science* **2005**, *307*, 397-400.

[15] K. Sumida, C. M. Brown, Z. R. Herm, S. Chavan, S. Bordiga, J. R. Long, *Chem. Commun.* **2011**, *47*, 1157-1159.

[16] M. K. Sharma, I. Senkovska, S. Kaskel, P. K. Bharadwaj, *Inorg. Chem.* **2011**, *50*, 539-544.

[17] Z. Xu, C. Li, X. Kang, D. Yang, P. Yang, Z. Hou, J. Lin, *J. Phys. Chem. C* **2010**, *114*, 16343-16350.

[18] D. B. Mitzi, *J. Chem. Soc. Dalton Trans.* **2001**, 1-12.

[19] **A. K. Vishwakarma**, P. G. Ghalsasi, A. Navamoney, Y. Lan, A. K. Powell, *Polyhedron* **2011**, *30*, 1565-1570.

[20] H. -L. Jiang, Q. Xu, *Chem. Commun.* **2011**, *47*, 3351-3370.

[21] P. Dechambenoit, J. R. Long, *Chem. Soc. Rev.* **2011**, *40*, 3249-3265.

[22] M. Kurmoo, *Chem. Soc. Rev.* **2009**, *38*, 1353-1379.

[23] M. Stöcker, *Micropor. Macropor. Mater.* **1999**, *29*, 3-48.

[24] F. J. Keil, *Micropor. Macropor. Mater.* **1999**, *29*, 49-66.

[25] C. Volkringer, T. Loiseau, N. Guillou, G. Férey, M. Haouas, F. Taulelle, N. Audebrand, I. Margiolaki, D. Popov, M. Burghammer, C. Riekel, *Cryst. Growth Des.* **2009**, *9*, 2927-2936.

[26] A. V. Neimark, F. -X. Coudert, A. Boutin, A. H. Fuchs, *J. Phys. Chem. Lett.* **2010**, *1*, 445-449.

[27] M. G. El-Shaarawy, *J. Mag. Mag. Mater.* **2000**, *217*, 94-98.

[28] D. Abdelaziz, A. Thrierr-Sorel, R. Perret, B. Chaillot, *Rev. Roum. Chim.* **1977**, *22*, 857-863.

[29] J. D. Martin, R. F. Hess, P. D. Boyle, *Inorg. Chem.* **2004**, *43*, 3242-3247.

[30] P. C. Moews, Jr., *Inorg. Chem.* **1966**, *5*, 5-8.

[31] T. B. Swanson, V. W. Laurie, W. Duffy, Jr., *J. Chem. Phys.* **1968**, *49*, 4407-4411.

[32] S. Bourrelly, B. Moulin, A. Rivera, G. Maurin, S. Devautour-Vinot, C. Serre, T. Devic, P. Horcajada, A. Vimont, G. Clet, M. Daturi, J. -C. Lavalley, S. Loera-Serna, R. Denoyel, P. L. Llewellyn, G. Férey, *J. Am. Chem. Soc.* **2010**, *132*, 9488-9498.

[33] M. Kurmoo, H. Kumagai, S. M. Hughes, C. J. Kepert, *Inorg. Chem.* **2003**, *42*, 6709-6722.

[34] D. A. Tucker, P. S. White, K. L. Trojan, M. L. Kirk, W. E. Hatfield, *Inorg. Chem.* **1991**, *30*, 823-826.

[35] G. Vyas, L. W. ter Haar, *J. Appl. Phys.* **1994**, *76*, 7111-7113.

[36] M. Wei, R. D. Willett, *Inorg. Chem.* **1995**, *34*, 3780-3784.